INTERNATIONAL JOURNAL OF AUTOMOTIVE AND MECHANICAL ENGINEERING
ISSN: 2229-8649 e-ISSN: 2180-1606
VOLUME 22, ISSUE 4, 2025, 12970 - 12985
DOI: https://doi.org/10.15282/ijame.22.4.2025.10.0987

RESEARCH ARTICLE

Energy Storage Configuration and Scheduling for Rail Transit Based on a Beetle Antennae-Optimized Back Propagation Neural Network Prediction Algorithm

Lidong Han*, Lei Yang, Lang Su

School of Mechanical & Electrical Engineering, Suzhou Global Institute, Suzhou, 215163, China

ABSTRACT – To meet the growing energy management needs of the rail transit system, this study explores the configuration and scheduling strategies of rail transit energy storage. An innovative prediction-allocation-dispatch co-optimization framework based on the deep fusion of the Beetle Antennae search algorithm and back-propagation neural network is proposed. This framework solves the problem of the co-optimization of renewable energy output uncertainty and the economy of energy storage. The study adopts a Beetle Antennae-optimized backpropagation neural network prediction algorithm to improve the prediction accuracy of wind and solar power generation. A hybrid energy storage configuration system is designed by comprehensively considering the energy storage life and cost, and a multi-time scale energy scheduling optimization scheme is proposed. The experiment showed that the optimization prediction algorithm could significantly improve prediction accuracy and had superior iterative optimization effects. Compared with traditional prediction algorithms, this optimization algorithm reduced the mean square error of photovoltaic and wind power prediction by 41.11% and 34.02% respectively and reduced the time consumption by 29.95% and 33.21% compared to other algorithms. Meanwhile, the hybrid model had significant advantages in energy storage costs and net benefits, with a total scheduling cost reduction of 17.95% compared to other energy storage systems and a response speed improvement of 13.98%. This indicates that the proposed optimization algorithm and configuration model can enhance the energy utilization function and scheduling flexibility of the rail transit system, supporting the sustainable development of rail transit.

ARTICLE HISTORY
Received : 06th Mar. 2025
Revised : 20th May 2025
Accepted : 11th Aug. 2025
Published : 16th Nov. 2025

KEYWORDS
Beetle antennae optimization algorithm
BP neural network
Rail transit
Energy storage configuration
Scheduling optimization

1. INTRODUCTION

In recent years, Urban Rail Transit (URT) has become an important component of urban transportation due to its benefits of large capacity and low pollution. The rapid development of URT has led to a continuous increase in operating mileage, and the electricity demand has also increased accordingly. The huge energy consumption problem and the imbalance between energy supply and demand during operation are becoming increasingly prominent. This not only imposes a heavy burden on operating costs but also poses challenges to the sustainable use of energy [1-3]. Therefore, exploring the application of Renewable Energy (RE) in URT to reduce grid load, lower energy consumption, and achieve green environmental protection is meaningful. However, the uncertainty and intermittency of RE generation pose challenges to its stable application in URT [4].

In this context, the importance of energy storage scheduling strategies for rail transit is increasingly deepening. On the one hand, reasonable energy storage scheduling can effectively balance fluctuations in energy supply and demand within the rail transit system, thereby improving energy utilization efficiency. On the other hand, Multi-Time Scale Energy Scheduling (MTSES) optimization schemes can better adapt to the operational characteristics of rail transit systems at different time scales, achieve refined energy management, further reduce operating costs, and improve system stability and reliability. Therefore, accurately predicting the output of RE and reasonably configuring an Energy Storage System (ESS) has become a hot and difficult topic in current research.

The existing prediction methods primarily utilize machine learning algorithms, including Back Propagation (BP) neural networks. However, improving prediction accuracy and stability remains significant [5-6]. The Beetle Antennae Search (BAS) algorithm, as an emerging intelligent optimization algorithm, is excellent in fast convergence velocity and strong global search capacity, providing new ideas for parameter optimization of BP networks [7]. Therefore, this study utilizes the BAS algorithm to enhance the BP network, taking into account economic effects and energy storage cycles to develop an energy storage configuration system, and proposes an MTSES strategy.

The purpose of the research is to improve the utilization rate of RE in URT, reduce operating costs, and minimize environmental impact through accurate energy prediction and efficient energy storage configuration. The innovation of this study lies in combining the BAS algorithm with the BP network and applying it to railway ESS, thereby overcoming the limitation of a single optimization objective. Through the collaborative design of the MTSES strategy and hybrid

*CORRESPONDING AUTHOR | L. Han | ✉ lidonghanld@outlook.com

energy storage configuration, the contradiction between the uncertainty of RE output and the energy storage economy is solved. This study provides a more accurate predictive basis for optimizing energy storage configurations and scheduling strategies in rail transit, offering new directions for subsequent related research.

There are four sections to study the overall structure. Section 1 summarizes the research achievements and shortcomings of various countries on Energy Storage Configuration Systems for Rail Transit (RT-ESCS) and BP networks. Section 2 designs the RT-ESCS system and multi-objective economic optimization model for the BP network prediction algorithm optimized by the BAS algorithm (BAS-BP). Section 3 conducts experiments and analysis on the proposed BAS-BP prediction algorithm and energy storage configuration system. Section 4 summarizes the experimental results and indicates future research directions.

2. RELATED WORKS

Currently, many scholars have conducted numerous explorations in RT-ESCS. To improve the voltage stabilization effects of fixed ESS, Liu et al. proposed a battery-supercapacitor hybrid ESS. By utilizing an adaptive energy management framework and power allocation strategy, the adaptability problem of two energy storage media to load changes has been addressed, thereby slowing down the battery decay rate [8]. To meet the electricity demand of URT and improve operational stability, Dong et al. proposed a multisource traction system configuration. This system combined traction systems, RE, and ESS to manage energy flow through coordinated control strategies, reducing peak power and voltage fluctuations in substations [9]. To recover the Regenerative Braking Energy (RBE) of high-speed railway locomotives and reduce system power consumption, Yuan et al. proposed an energy management strategy of adding a hybrid ESS and installing rooftop photovoltaics based on the interconnection between the station and traction power system. This strategy significantly reduced the operating costs of railway systems by optimizing scheduling models and employing mixed-integer linear programming methods [10].

To improve the utilization efficiency of RBE and alleviate the problem of voltage imbalance, Chen et al. proposed a dynamic voltage imbalance adjustment strategy based on day-ahead prediction information. It utilized the power flow allocation constraint set converted into the traction power supply system, reducing system operating costs and improving the utilization efficiency of RBE and the cycle life of energy storage devices [11]. To reduce the circuit and control complexity caused by voltage differences between battery cells and supercapacitor cells in hybrid ESS, Xu et al. proposed a bidirectional integrated equalizer built on a single-ended primary inductor converter. It reduced the complexity of hybrid ESS by balancing multi-winding transformers and generating current ripple drives [12].

In prediction algorithms, BP networks are widely utilized due to their powerful nonlinear mapping ability. Li et al. designed an optimized BP system as a financial warning model to address the financial risks faced by enterprises. By describing its working principle, reasoning process, analyzing its shortcomings, and proposing solutions, it has achieved high accuracy in predicting the financial difficulties of listed companies, proving the effectiveness of optimizing the BP network [13]. To standardize the evaluation criteria for second-hand car prices and enhance the accuracy of price prediction, Liu E et al. proposed a second-hand car price prediction method based on Particle Swarm Optimization (PSO) and Grey Correlation Analysis (GCA) combined with a BP network. It filtered and optimized vehicle parameters and other feature variables through GCA and PSO algorithms, achieving higher prediction accuracy than traditional models and providing new ideas for used car evaluation [14]. Bai et al. proposed a high-precision prediction model for temperature control of drying units. It improved the BP network by utilizing the grey wolf optimizer to enhance the model's correlation, and employed the projection conjugate gradient method for nonlinear optimization to improve convergence speed and control effectiveness [15]. Deng et al. proposed a power load forecasting model based on the genetic algorithm and BP, along with a remote management scheme for Energy Storage Power Plants (ESPPs) driven by the metaverse, to satisfy the requirement for high-precision power load forecasting in ESPP systems. This scheme realized the transformation of ESPP from relying on simulation-based management and control to relying on smart management [16].

In summary, although fruitful research results have been achieved in RT-ESCS and scheduling optimization, there is still room for improving the accuracy of energy prediction and the rationality of configuration, as more attention is paid to a single optimization objective. Therefore, this study designs a comprehensive energy storage configuration system and scheduling scheme based on the BAS-BP algorithm to lift energy utilization efficiency and reduce operating costs. The innovation lies in the design of the BAS-BP algorithm, which utilizes BAS to optimize the BP network and improve energy prediction precision. A comparison of the findings of different RT-ESCSs and prediction algorithms is shown in Table 1.

Table 1. Comparison of research results on energy storage configuration and scheduling optimization methods for different rail transit systems

References	Research methods	Key findings	Weaknesses
Liu Y et al. [8]	Adaptive energy management framework and power distribution strategy	Delay the attenuation rate of the battery and reduce the power fluctuation	No consideration is given to multi-time scale scheduling
Dong H et al. [9]	Multisource traction system integrating traction system, RE and ESS	Reduce the peak power and voltage fluctuation of the substation, improve the operation stability	The impact of unquantified energy storage life on the economy is not considered
Yuan et al. [10]	Mixed integer linear programming	Reduce the operating costs of the railway system	Unable to cope with second-level power fluctuation requirements
Chen Y et al. [11]	A dynamic voltage imbalance regulation strategy based on the prediction of the day	Improve the energy utilization rate of regenerative braking and extend the life of energy storage devices	There is a risk of power imbalance in the RE fluctuation scenario
Xu et al. [12]	Bidirectional integrated equalizer based on a single-end primary inductor converter	Reduce the circuit and control complexity of hybrid ESSs	The total life cycle cost is higher than that of traditional solutions
Li et al. [13]	Optimize BP neural network to build a financial early warning model	The accuracy of financial distress prediction of listed companies has been significantly improved	The impact of real-time data updates on predictions is not considered
Liu E et al. [14]	A method of used car price prediction based on PSO-GCA-BP network	The prediction accuracy is higher than the traditional model	The multi-objective optimization problem is not solved, and the model complexity is high
Bai et al. [15]	The BP neural network is improved by using the gray wolf optimizer	Improve the convergence speed of the prediction model and reduce the temperature control error	It cannot meet the real-time scheduling requirements
Deng et al. [16]	A genetic algorithm-BP neural network power load forecasting model is constructed	Improve the accuracy of load forecasting	The high complexity of multi-objective optimization leads to an increase in scheduling delay

3. METHODOLOGY

The study first constructs an RT-ESCS model, designs a hybrid battery-ultracapacitor energy storage architecture that considers energy storage lifetime and economic constraints, and quantifies system performance using the rainfall counting method and whole-life cycle cost modeling. Secondly, a BAS-BP prediction algorithm is proposed to improve the accuracy and convergence efficiency of wind and light output prediction. Finally, an improved PSO algorithm is used to solve the energy storage allocation model, and a real-time MTSES scheme is designed to achieve the dual optimization of power fluctuation smoothing and economic objectives.

3.1 Design of RT-ESCS Model

3.1.1 Hybrid energy storage system architecture

Wind and Solar Power (WASP) generation is characterized by intermittency and volatility, and its power prediction is a crucial link to achieving a stable energy supply. While the rail transit system's operating load changes dynamically over time and with passenger flow, accurately grasping its load demand law is the basis for guaranteeing the reliability of power supply. Therefore, based on the power prediction of wind power generation and the load demand of rail transit, the study constructs an RT-ESCS model, whose basic structure is shown in Figure 1.

In Figure 1, the collected wind speed, wind direction, light intensity, historical WASP generation data, as well as train traction power demand, operating schedule, and other information are first input into the system. Then, the BAS-BP prediction algorithm is utilized to forecast the wind and PV power generation. It is assumed that meteorological factors primarily influence wind power and that historical data can accurately reflect future power generation trends. It is also assumed that the ESS has sufficient response speed and stability to meet the rapid changes in power demand associated with rail transportation.

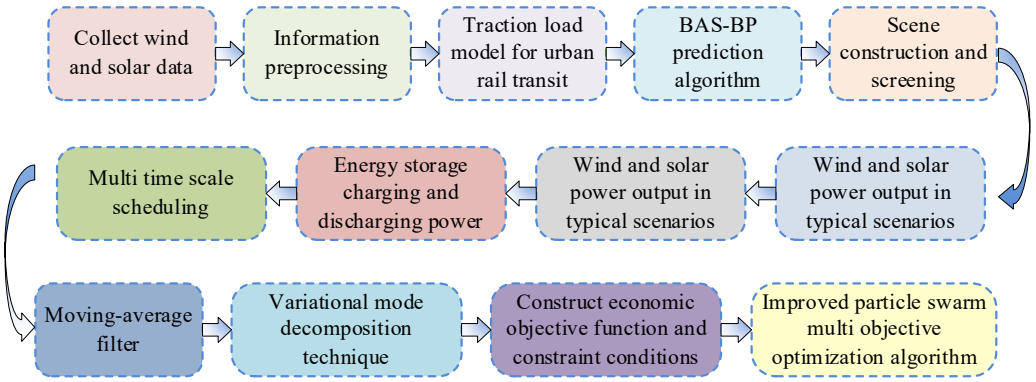

Figure 1. Basic structure of a hybrid railway energy storage configuration system

The final output of wind power prediction values, the Charging and Discharging (C&D) power of ESS, the State of Charge (SOC) change curves of batteries and supercapacitors, and the grid interaction power cover the power fluctuations of solar power generation and the output changes of wind power generation. By predicting the traction power data, the power demand of the train at different operating stages can be accurately grasped. In Figure 1, the system collected past meteorological information and vehicle departure time and used the BAS-BP algorithm to predict wind and photovoltaic power generation, covering the power fluctuations and output changes of WASP. Meanwhile, the traction power data are predicted to accurately grasp the power demand of the train at different operating stages.

3.1.2 Modelling of storage lifetime and economics

Based on this, the study designs a power plan for energy storage C&D and optimizes energy storage scheduling across multiple time scales. The grid-connected power is stabilized through sliding average filtering and variational mode decomposition techniques. Among them, this study uses the rain flow counting method to calculate the lifespan and annual replacement frequency of the battery [17], as shown in Eq. (1).

$$\begin{cases} L = \sum_j^n L\left(A_{DoD,j}\right) \\ D = \frac{L}{U(A_{DoD,j})} \\ R = \sum_{j=1}^{365} \sum_{h=1}^{18} \frac{D(j)}{2} - 1 \end{cases} \tag{1}$$

In Eq. (1), L is the number of equivalent cycles of the battery under specific operating conditions. D is the amount of capacity lost during battery use. R is the replacement frequency of the battery. U is the cycle life at different discharge levels. n is the gross number of cycles. j and h are indices of the number of days and time periods in a day. $A_{DoD,j}$ is the discharge depth of the battery. After determining the service life of the ESS, sliding average filtering is used to process non-stationary signals. The signal is smoothed by calculating the average value within a fixed-size window, which suppresses noise and random fluctuations. At the same time, the variational mode decomposition technique is employed to decompose the fluctuating power into high- and low-frequency components. The frequency center and bandwidth of each component are determined by iteratively searching for the optima of the variational model, which enables adaptive frequency domain partitioning of the signal and effective separation of each component [18-19]. The final expression for the reconstructed signal is shown in Eq. (2).

$$\begin{cases} G_{high} = \sum_{v=1}^{\delta} r_v \\ G_{low} = \sum_{v=\delta+1}^{\delta} r_v \end{cases} \quad ,\delta \in 1,2,\ldots,m \tag{2}$$

In Eq. (2), G_{high} and G_{low} are the high-frequency subsequence reconstruction power and the low-frequency subsequence reconstruction power. δ is the segmentation point for modal components, used to distinguish between high and low frequency components. m is the number of variational modal component sequences. v is the total number of modal components. r_v is the residual Wiener filter. After completing power smoothing, this study further examines the full life cycle cost of the ESS, comprehensively considering factors such as government subsidies and related benefits, as well as the economic benefits of power grid interaction, to establish a multi-objective economic optimization model. After completing power smoothing, this study further considers factors such as the full lifecycle cost of ESS, government subsidies and related benefits, and the economic benefits of grid interaction, and establishes a multi-objective economic optimization model. The economic objective function is shown in Eq. (3).

$$\begin{cases} F_1 = \left(\frac{(1+\eta)^{\mu}-1}{\eta(1+\eta)^{\mu}} C_y + \frac{1}{(1+\eta)^{\mu}} C_c + C_t\right)/\mu \\ F_2 = -E_b - E_z - E_q \\ F_3 = -E_d - C_h + C_b + C_g \end{cases} \tag{3}$$

In Eq. (3), F_1 means the life cycle cost function of energy storage. F_2 is the function of economic subsidies and related benefits. F_3 is the lifecycle of the ESS. η is the discount rate used to calculate the present value of future cash flows. μ is the energy economy function of grid interaction. C_y denotes the operation and maintenance cost. C_c and C_t are the disposal and investment costs. E_b is a subsidy profit. E_z represents the time and space allocation and utilization efficiency of RE. E_q is the economic return of substation renovation. E_d is the benefit of purchasing and selling electricity in the power grid. C_h is the cost of the SOC. C_b is the cost of purchasing electricity from the grid for the ESS. C_g means the expenditure of over C&D energy storage. In hybrid ESS, the C&D power allocation strategies of batteries and ultracapacitors are based on their respective dynamic response characteristics and the technical limitations of the storage medium. Specifically, low-frequency power fluctuation components, such as the power demand resulting from long-term trend changes in rail transit base loads and wind power generation, are absorbed by the battery. The high-frequency components, such as train braking energy recovery and short-term random fluctuations of wind power generation, are handled by supercapacitors. After the grid-connected power is decomposed in the frequency domain using the variational modal decomposition technique, the low-frequency component is smoothed by sliding average filtering and fed into the battery C&D controller, while the high-frequency component is directly routed to the supercapacitor C&D circuit. The update rules for the SOC of batteries and capacitors under different C&D states are shown in Eq. (4).

$$\begin{cases} H_b=\frac{H_b(t-\Delta t)-P_b(t)\Delta t\lambda_b}{Z_b}, P_b<0 \\ H_c=\frac{H_c(t-\Delta t)-P_c(t)\Delta t\lambda_c}{Z_c}, P_c\geq 0 \\ H_b=\frac{H_b(t-\Delta t)-P_b(t)\Delta t}{\lambda_b Z_b}, P_b<0 \\ H_c=\frac{H_c(t-\Delta t)-P_c(t)\Delta t}{\lambda_c Z_c}, P_c\geq 0 \end{cases} \tag{4}$$

In Eq. (4), H_b and H_c are the SOCs of the battery and the capacitor. t means time. Δt is the time increment. λ_b and λ_c are the C&D efficiencies of batteries and capacitors. P_b and P_c are the rated power of batteries and capacitors. Z_b and Z_c are the nominal capacities of batteries and capacitors. The constraint condition for the C&D power of batteries and capacitors reaching the upper limit of the SOC is shown in Eq. (5).

$$\begin{cases} P_b(t)=Max\{-P_{b,r},-P_d(t),(H_b(t-\Delta t)-H_{bMax})Z_b/\Delta t\lambda_b\} \\ P_c(t)=Max\{-P_{c,r},-P_d(t),(H_c(t-\Delta t)-H_{cMax})Z_c/\Delta t\lambda_c\} \end{cases} \tag{5}$$

In Eq. (5), $P_{c,r}$ and $P_{b,r}$ are the nominal power of the capacitor and battery. $P_d(t)$ is the battery C&D command power. H_{bMax} and H_{cMax} are the maximum SOC for batteries and capacitors. The constraint condition for the C&D power of batteries and capacitors reaching the lower limit of the SOC is shown in Eq. (6).

$$\begin{cases} P_b(t)=Min\{P_{b,r},P_d(t),(H_b(t-\Delta t)-H_{bMin})Z_b\lambda_b/\Delta t\} \\ P_c(t)=Min\{P_{c,r},P_d(t),(H_c(t-\Delta t)-H_{cMin})Z_c\lambda_c/\Delta t\} \end{cases} \tag{6}$$

In Eq. (6), H_{bMin} and H_{cMin} denote the minimum SOC of the battery and capacitor. During the real-time scheduling phase, the energy storage management system ensures that the charge state is always within the safety threshold by dynamically adjusting the C&D power priorities. The above constraints ensure that the ESS operates within a safe and effective range, preventing over-charging or over-discharging, thereby extending the service life of the energy storage equipment.

3.2 Design of Prediction Algorithm Based on BSA-Optimized BP Network

3.2.1 Basic structure of BP network

After completing the design of the hybrid RT-ESCS model, the study proposes the BAS-BP algorithm to predict the wind and light processing. The BP network learns the relationship between historical meteorological conditions and wind power, continuously adjusting network parameters such as weights and biases through forward propagation and backpropagation to minimize the error between predicted and actual WASP values. Therefore, accurate prediction of WASP has been achieved, and its basic structure is displayed in Figure 2 [20].

In Figure 2, the network mainly has three layers: the input layer, the hidden layer, and the output layer. After inputting meteorological data, including wind speed and direction, temperature, and light intensity into the hidden layer, the input is processed through weighted summation and nonlinear activation functions. During the training process, obtaining parameters through random initialization can lead the BP network to become stuck in a local optimal solution.

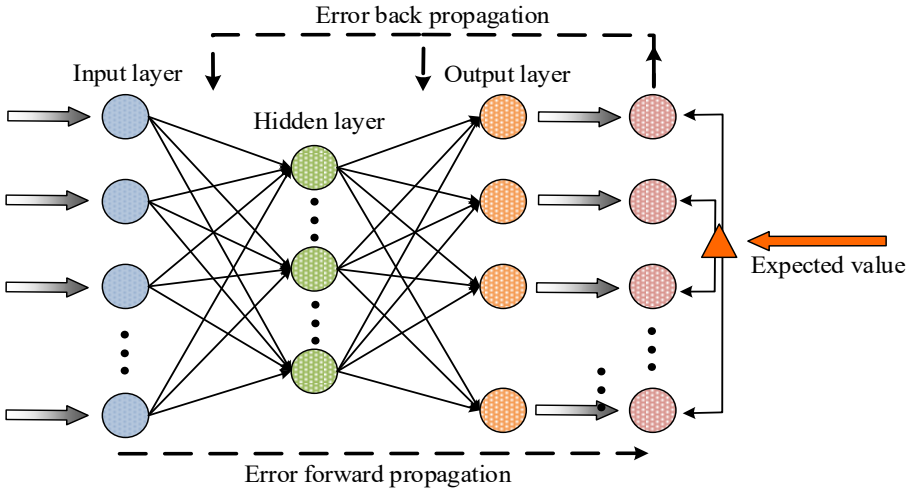

Figure 2. Basic structure of BP network

2.2.2 Integrated optimization process of BAS-BP

To improve prediction accuracy, this study uses the BAS to perfect the thresholds and weights of the BP network. The structure of the optimized prediction algorithm is exhibited in Figure 3.

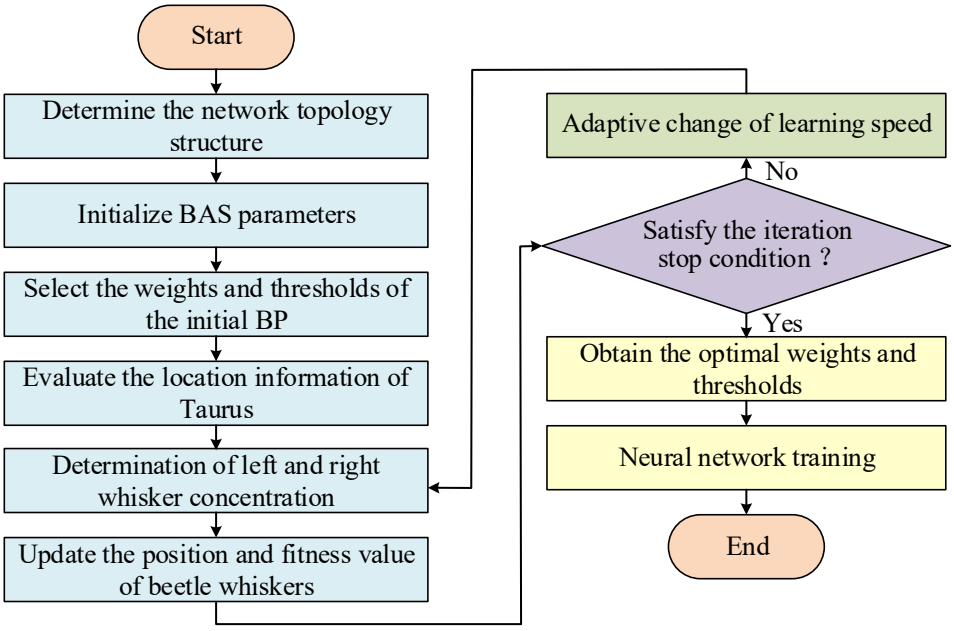

Figure 3. BAS-BP prediction algorithm operation procedure

According to Figure 3, this study uses BAS to preliminarily screen the parameters of BP. The weights and thresholds of the BP network are used as parameters to be optimized in BAS to construct a fitness function. An iterative search is then performed until the optimal solution of the BP network weights and thresholds is obtained. Firstly, a random vector oriented towards the Beetle Antennae is created, and a random number is selected as the initial position of the BAS, as shown in Eq. (7) [21].

$$\vec{O}=\frac{rands(s,1)}{\|rands(s,1)\|} \tag{7}$$

In Eq. (7), $\vec{O}$ is the initial direction of the beetle. s is the spatial dimension for beetles to forage. $rands(s,1)$ is a random vector. After determining the initial position of the beetle, the Mean Squared Error (MSE) of the BP on the training set is selected as the fitness evaluation function, as expressed in Eq. (8).

$$MSE=\frac{1}{N}\sum_{k=1}^{N}(x_k-y_k)^2 \tag{8}$$

In Eq. (8), N and k are the number of samples and the sample index in the training set. x_k and y_k are the output and actual values of sample k. After obtaining the fitness function, the left and right directions of the beetle's antennae are continuously changed for search. The calculation of the Beetle Antennae's position after changing direction is shown in Eq. (9) [22].

$$\begin{cases} S_a=S^i+d^i\vec{O} \\ S_b=S^i-d^i\vec{O} \end{cases} \tag{9}$$

In Eq. (9), S_a and S_b are the positions of the two antennae of the beetle. S^i is the current position of the Taurus. d is the distance between two antennae. i is the number of iterations for position change. The fitness function values of the beetle are calculated and compared according to Eq. (9), and the beetle position is updated based on network errors, as given by Eq. (10) [23].

$$S^i=S^{i-1}+l^i\vec{O}sign\left(f(S_a-S_b)\right) \tag{10}$$

In Eq. (10), S^{i-1} is the position of the Taurus in the previous iteration. l is the iteration step size. $\vec{O}sign\left(f(S_a-S_b)\right)$ is a sign function that determines the direction of the Taurus based on the difference in function values between S_a and S_b. The value of the current position of the Taurus is calculated, and it is determined whether the fitness value at this time meets the iteration stop condition. If the conditions are met, the optimal output is required; Otherwise, the iteration will continue by changing the position of the beetle. Finally, the obtained optimal weights and thresholds are fed into the BP for training, completing the prediction task.

3.3 Solution and Scheduling Optimization of the RT-ESCS Model

3.3.1 Improved multi-objective PSO algorithm

Based on the previously designed orbital energy storage configuration model that considers energy storage life and economy, this study utilizes an improved multi-objective PSO algorithm to solve the energy storage economic optimization problem, as shown in Figure 4.

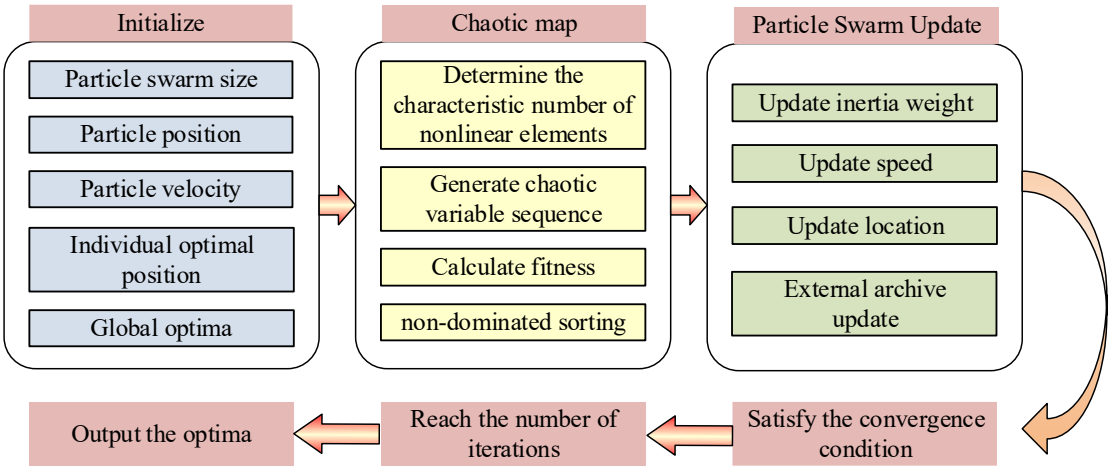

Figure 4. Improved multi-objective PSO algorithm flow

In Figure 4, this study enhances the inertia weight update strategy of the multi-objective PSO algorithm. It introduces a chaotic search mechanism to improve the algorithm's optimization ability and convergence speed, thereby avoiding local optima and achieving the optimal energy storage configuration scheme. The expression for the nonlinear, decreasing adaptive inertia weight is shown in Eq. (11).

$$w=w_{Min}+e^{(-(20\varepsilon/\varepsilon_{Max})^2)}(w_{Max}-w_{Min}) \tag{11}$$

In Eq. (11), w is the inertia weight. w_{Min} and w_{Max} are the minimum and maximum values of inertia weights. ε is the number of iterations at this moment. ε_{Max} is the maximum iteration.

2.3.2 Multi-timescale scheduling optimization

Finally, this study proposes an MTSES optimization scheme based on the temporal features of energy supply and demand in rail transit, as illustrated in Figure 5. In Figure 5, in the day-ahead dispatching phase, the time-sharing price and demand-side response are considered, and the economic optimization model is established based on the forecasted wind power generation and rail transit load demand, with the hour as the time scale. By optimizing the objective functions such as generation and regulation costs, energy storage costs, and wind curtailment costs, and meeting the constraints such as wind turbine unit output, energy storage power, and SOC, the day-ahead scheduling plan is obtained. During the intra-day scheduling phase, the predictive model is utilized, with minutes as the time scale, and the Latin hypercube sampling method is used to obtain WASP supply data in multiple scenarios. Combined with actual supply and demand data and prediction error fluctuations, rolling optimization is carried out. By establishing the state balance equation and objective function, and considering the constraints such as active power balance, energy storage charging state, and tie line power, the day-ahead scheduling plan is constantly revised to address the uncertainty of RE. In the real-time scheduling phase, a train scheduling energy optimization model is established based on the real-time operating status and

energy-saving control strategy of URT trains, with a time scale of seconds. Considering the mechanical characteristics, operating conditions, and power consumption analysis of the train, combined with the constraints of the C&D characteristics of the hybrid ESS, the real-time balance and efficient utilization of energy have been achieved by optimizing the train operation strategy and energy storage C&D strategy. Given the real-time operational data, the intra-day scheduling plan has been revised in reverse.

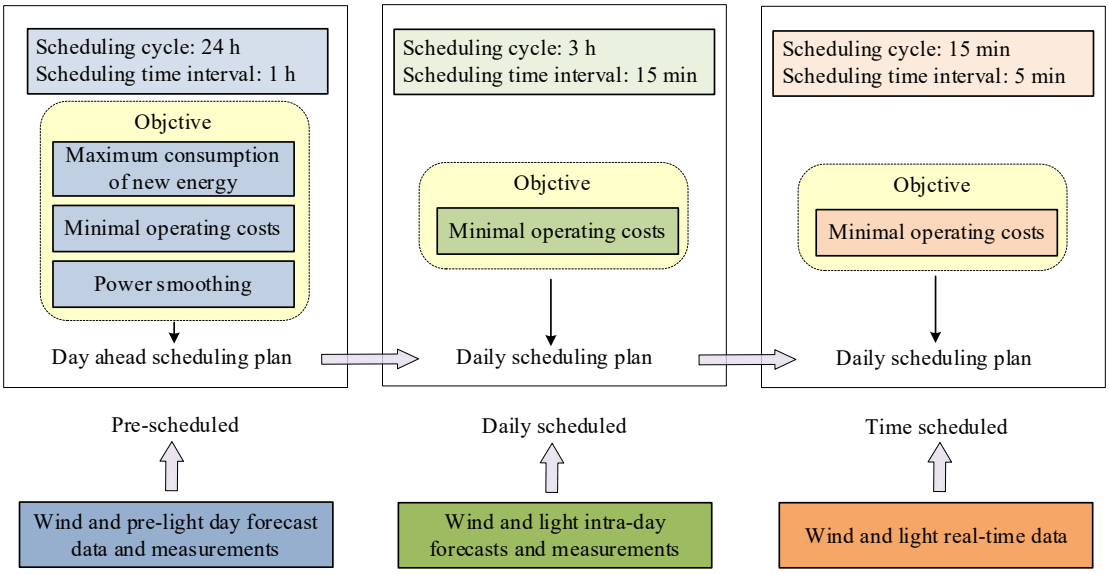

Figure 5. Optimization steps for MTSES

4. RESULTS

This study first validated the performance of the BAS-BP. Secondly, this study validated the RT-ESCS model considering the energy storage cycle and cost and analyzed the optimization scheduling results.

4.1 Experimental Parameters and Verification of the BAS-BP Algorithm

To verify the effectiveness of the proposed BAS-BP prediction algorithm and RT-ESCS model, the study designs simulation experiments. The experimental data were collected from the real-time monitoring system of a URT line, encompassing environmental parameters such as minute-level wind speed and light intensity recorded at the weather station, as well as historical output data from photovoltaic and wind turbines. At the same time, it integrates the departure moments, traction power curves, and hourly passenger flow statistics from the train operation log to ensure the temporal and spatial consistency of the multisource information.

Table 2. The parameters of supercapacitors and batteries used in the energy storage configuration model

Parameter	Supercapacitor parameters	Battery parameters
Upper limit of SOC	0.80	0.90
Lower limit of SOC	0.10	0.20
Rated capacity (kWh)	500	2000
Maximum charging power (kW)	200	100
Maximum charging power (kW)	200	100
Unit capacity cost (yuan·kwh-1)	0.05	0.05
Unit power cost (yuan·kw-1)	26000	2200
Unit capacity scrap disposal cost (yuan·kwh-1)	0.04	0.06
Unit power scrap disposal cost (yuan·kw-1)	0.51	0.65
C&D efficiency (%)	90	95
Operation and maintenance cost coefficient (yuan·kWh·year)	0.02	0.10
Power grid purchase cost (yuan·kWh)	0.45 (peak time)	0.45 (peak time)
	0.30 (normal)	0.30 (normal)
	0.20 (valley time)	0.20 (valley time)

The data preprocessing stage uses linear interpolation to fill in the missing segments, maps all features to the 0 to 1 interval by min-max normalization, and eliminates scale differences between different magnitude parameters, such as wind speed

and power. The initial learning rate is set to 0.001, and the batch size is 64. All numerical simulations are implemented on a 64-bit PC with a 1.70 GHz CPU, and calculations are performed using the Yalmip toolbox and the Gurobi algorithm package in MATLAB. Table 2 shows the parameters of supercapacitors and batteries used in the energy storage configuration model.

This study first verifies the effectiveness of the BAS-BP algorithm by introducing a BP network, Time Series (TS), and Convolutional Neural Network (CNN) to design performance comparison experiments. Among them, the BP network simulates the connection relationship between human brain neurons, learns from historical data, and predicts wind power generation by adjusting the weights and biases between neurons. The TS prediction algorithm predicts future power generation by analyzing the temporal trends and cyclical patterns of historical data, utilizing the statistical properties of time series data. The CNN prediction algorithm automatically extracts local features from data through convolutional layers and is suitable for processing data with spatial or temporal local correlations. The predictive ability of four algorithms for photovoltaic and wind power output during the same period from 6:00 am to 6:00 pm on the same day is compared, as shown in Figure 6.

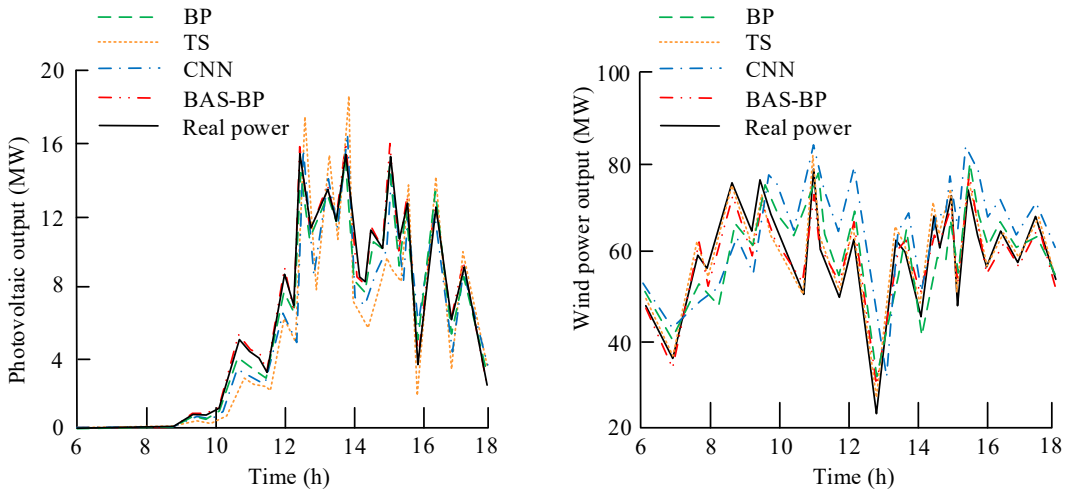

(a) Comparison of photovoltaic output forecast results (b) Comparison of wind power output forecast results

Figure 6. Comparison of four algorithms' outgoing power prediction capabilities for photovoltaics and wind power

Figure 6 (a) compares the predictive ability of different algorithms for photovoltaic output. The prediction errors of CNN and TS are relatively large, while the BAS-BP prediction results are closest to the actual power generation, and its prediction accuracy is significantly improved compared to BP. For example, at 10:00 am, the BP algorithm predicts a value of 0.83 MW, while the actual value is 0.96 MW, resulting in an error of 13.54%. The BAS-BP algorithm predicts a value of 0.97 MW, with an error of only 1.04%. Based on Figure 6(b), TS achieves the best performance in wind energy prediction, which may be due to the fact that wind power is a continuous variable with large fluctuations and exhibits a temporal relationship. The prediction accuracy of BAS-BP is slightly lower than that of TS. However, it still has significant advantages compared to CNN and BP, indicating that the introduction of BAS effectively improves the prediction performance of the BP network. Specifically, at 12:00, the BP algorithm predicts 69.42 MW, while the actual value is 65.93 MW, resulting in an error of 5.29%. The BAS-BP algorithm predicts 66.43 MW, with an error of 0.76%. Figure 6 shows that the prediction results of the BAS-BP algorithm at different time points are closest to the actual value, and the error rate is significantly lower than that of other algorithms. This difference mainly stems from the optimization mechanism of the BAS-BP algorithm. This algorithm simulates the foraging behavior of poplar trees and dynamically adjusts the weights and thresholds of BP to more accurately fit the trend of wind power generation. Meanwhile, this study compares the prediction iterations of four algorithms, as shown in Figure 7.

In Figure 7, CNN has the slowest iteration speed, is most prone to getting stuck in local optima, and ultimately maintains a low level of prediction performance. BAS-BP has the best convergence effect in photovoltaic and wind energy prediction, achieving optimal training results in about 80 iterations. Compared with other algorithms, BAS-BP has the lowest possibility of falling into local optima. This suggests that utilizing BAS to optimize BP networks is a reliable and reasonable approach, and BAS-BP exhibits superior convergence speed and predictive performance. On this basis, this study further validates the effectiveness of BAS-BP in balancing prediction accuracy and efficiency, as shown in Figure 8.

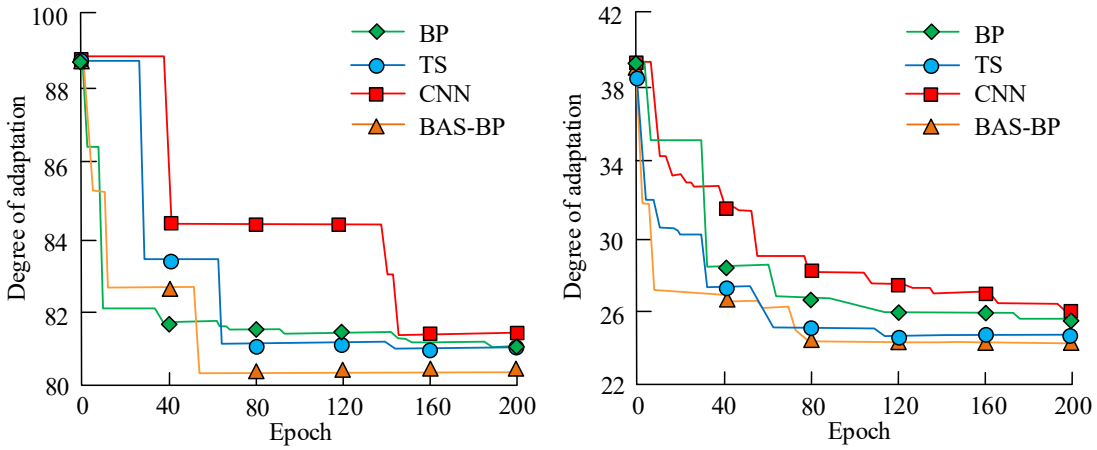

(a) Iterative comparison of photovoltaic forecasts (b) Iterative comparison of wind energy forecasts

Figure 7. Comparison of photovoltaics prediction and wind prediction iterations for four algorithms

Figure 8(a) shows the comparison of MSE values between photovoltaic and wind power prediction results using four algorithms. The MSE values of the BAS-BP algorithm for photovoltaic and wind power prediction are 36.57% and 40.18%, which are reduced by an average of 41.11% and 34.02% compared to other algorithms. In Figure 8(b), BAS-BP also exhibits a significant advantage in prediction time, with an average reduction of 29.95% and 33.21% in the time required for photovoltaic and wind power predictions, respectively, compared to other algorithms. This indicates that BAS-BP outperforms other algorithms in terms of prediction accuracy and also has significant advantages in computational efficiency, enabling it to complete prediction tasks in a shorter time. On this basis, to assess the model's robustness to key parameters, the study conducts a sensitivity analysis of the predicted parameters of the BAS-BP algorithm. The performance of the algorithm is compared for different BAS algorithm steps, and the results are shown in Figure 9.

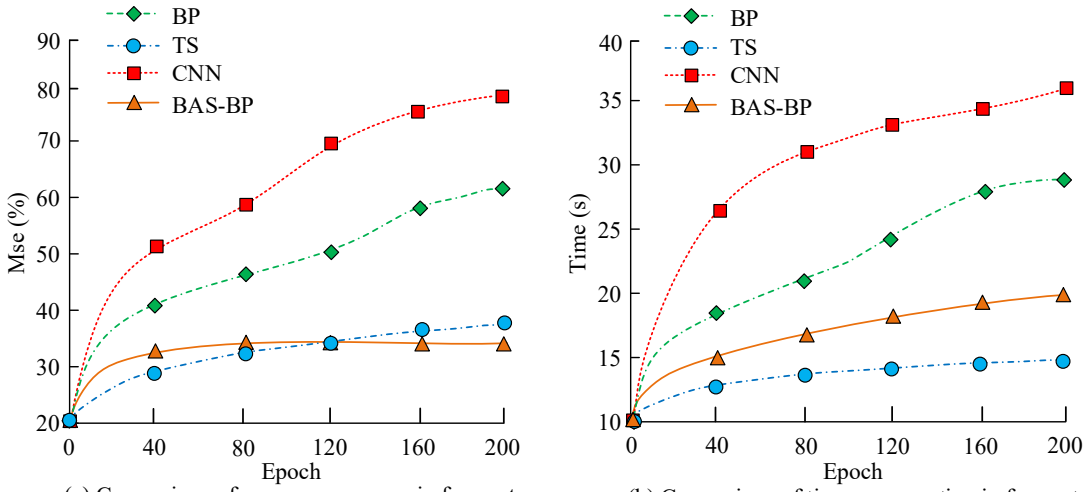

(a) Comparison of mean square error in forecast (b) Comparison of time consumption in forecast

Figure 8. Comparison of MSE and time consumption of four algorithms for predicting results

Figure 9(a) shows the change curve of the prediction accuracy of the BAS-BP algorithm under different step lengths. With the increase in the number of experiments, the prediction accuracies of all step lengths show an increasing trend, but the accuracy of step length 0.1 is always at the highest level. When the number of experiments reaches 500 times, the accuracy of step size 0.1 is 92.28%, while step size 0.4 is only 86.45%. This suggests that smaller step sizes allow the algorithm to more accurately tune the network parameters, thereby improving the prediction accuracy. Comparatively, a larger step size may cause the algorithm to skip the optimal solution during the parameter adjustment process, th ereby affecting the prediction accuracy. Meanwhile, combining with Figure 9(b), with the increase of the number of experiments, the computation time of all step lengths shows an increasing trend. The smaller the step length is, the slower the computation time grows. When the number of experiments is 500, the computation time of step size 0.1 is 95.46s, while that of step size 0.4 is 119.43s. This indicates that although smaller step sizes require more iterations to achieve higher prediction accuracy, the overall computation time growth is slower due to smaller adjustments per iteration and relatively lower computational complexity.

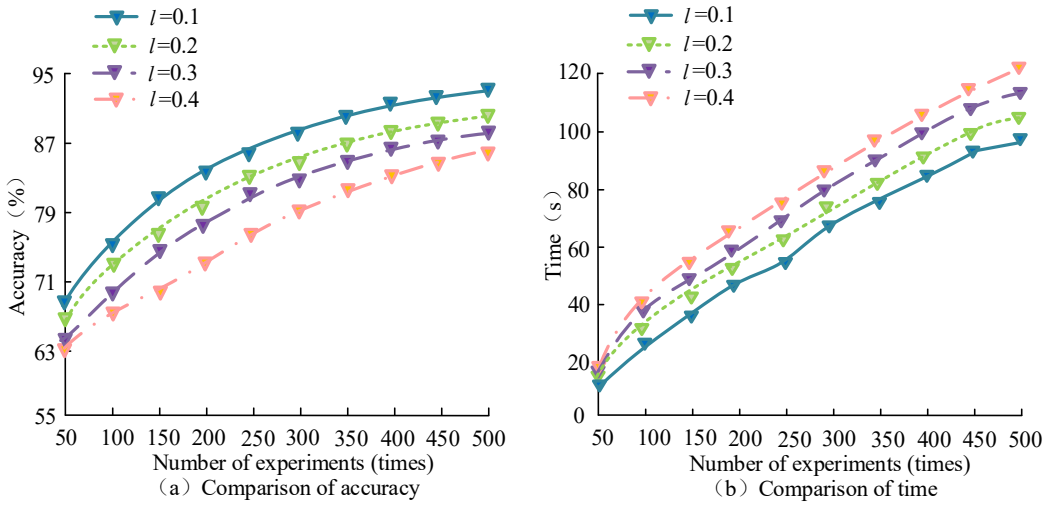

Figure 9. Comparison of prediction accuracy and prediction time of BAS-BP algorithm under different step lengths

Comparatively speaking, although a larger step size may quickly approach the optimal solution in the early stage, it may lead to an increase in computational complexity due to the larger adjustment of each iteration, thereby making the computational time grow faster. Taken together, the BAS-BP algorithm is sensitive to the step size, and it is necessary to balance the prediction accuracy and computational efficiency when choosing the step size to achieve the optimal performance. Finally, to further validate the generalization ability of BAS-BP and comprehensively evaluate its performance advantages, this study conducts 30 independent runs on BAS-BP. The performance indicators, such as MSE, runtime, and resource utilization, are recorded for each experiment, and their mean and standard deviation are calculated. The Long Short-Term Memory Network (LSTM), Gated Recurrent Unit (GRU), and Transformer models are also introduced as benchmarks, while the hybrid models of BP Network Based on PSO (PSO-BP) and BP Network Based on Genetic Algorithm (GA-BP) are introduced for comparison experiments. The results are shown in Table 3.

Table 3. Comparison of multiple running results of different algorithms

Index	LSTM	GRU	Transformer	BAS-BP	PSO-BP	GA-BP
Photovoltaic forecast MSE (%)	42.31 ± 1.45	44.12 ± 1.72	45.63 ± 2.01	36.57 ± 1.23	45.82 ± 1.89	50.13 ± 2.15
Wind power forecast MSE (%)	48.25 ± 1.68	49.87 ± 1.93	51.42 ± 2.34	40.18 ± 1.57	52.64 ± 2.12	58.91 ± 2.47
Training duration (s)	298.31 ± 10.2	212.58 ± 8.7	532.14 ± 15.3	95.46 ± 3.21	142.39 ± 5.1	183.25 ± 6.8
Converge the number of iterations	150	135	200	80	112	135
Hardware resource usage (GB of memory)	4.2	3.5	8.7	1.1	1.3	1.4

In Table 3, the BAS-BP model shows significant advantages in prediction accuracy, computational efficiency, and resource consumption. In the photovoltaic and wind power prediction tasks, the MSE values of BAS-BP are 36.57% and 40.18%, respectively, which are lower than those of the LSTM's 13.6% and 16.7% and Transformer's 19.9% and 21.9%, which verifies its good prediction accuracy. In terms of training time, BAS-BP takes only 95.46 s, which is 32%, 45%, and 18% of the time consumed by LSTM, GRU, and Transformer, respectively, highlighting the high efficiency of the algorithm. The hardware memory occupies 1.1 GB, indicating that its lightweight feature is suitable for edge computing scenarios. In addition, the number of convergence iterations of BAS-BP is 80, which is 28.6% and 40.7% less than PSO-BP and GA-BP, further reflecting its fast optimization capability. Experiments have shown that the use of BAS-BP effectively improves the power prediction accuracy of wind power generation, enabling ESS to more accurately match the power demand of rail transit. This lays the foundation for reducing unnecessary storage capacity allocation and operating costs, which is a key factor in reducing scheduling costs.

4.2 RT-ESCS and Scheduling Effectiveness Verification

Based on the relevant parameters of energy storage configuration, this study further analyzes the effectiveness of the RT-ESCS and scheduling method based on BAS-BP. Figure 9 shows the C&D power and SOC of the model. In Figure 10(a), the output power of the battery is relatively small, and because the C&D power of the battery is the low-frequency component of the load power, the output power is also relatively smooth. The output power of supercapacitors fluctuates greatly and frequently, indicating that supercapacitors can quickly perform C&D operations and meet the changing requirements of high-frequency power. In Figure 10(b), both the SOC of the supercapacitor and the battery satisfy the constraint conditions.

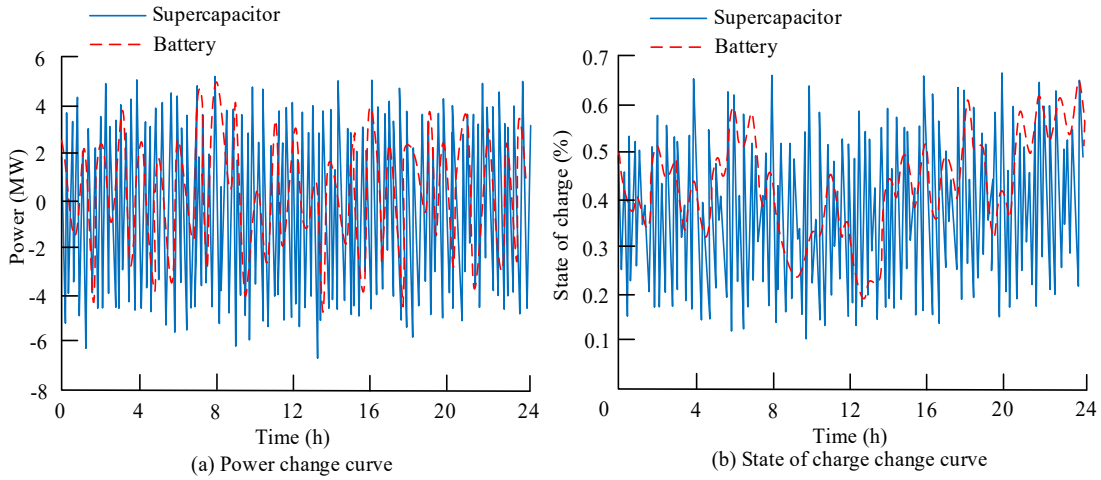

Figure 10. Charge discharge power and SOC variation curve of energy storage model

The small number of C&D cycles of the battery is beneficial for extending its service life, and the SOC at the beginning and end of the battery's operating cycle is equal, which can achieve long-term recycling. This study compares ESSs proposed by other scholars (References 6, 8, and 18) and analyzes the economic optimization effects of the RT-ESCS model under different passenger flow rates, as shown in Figure 11.

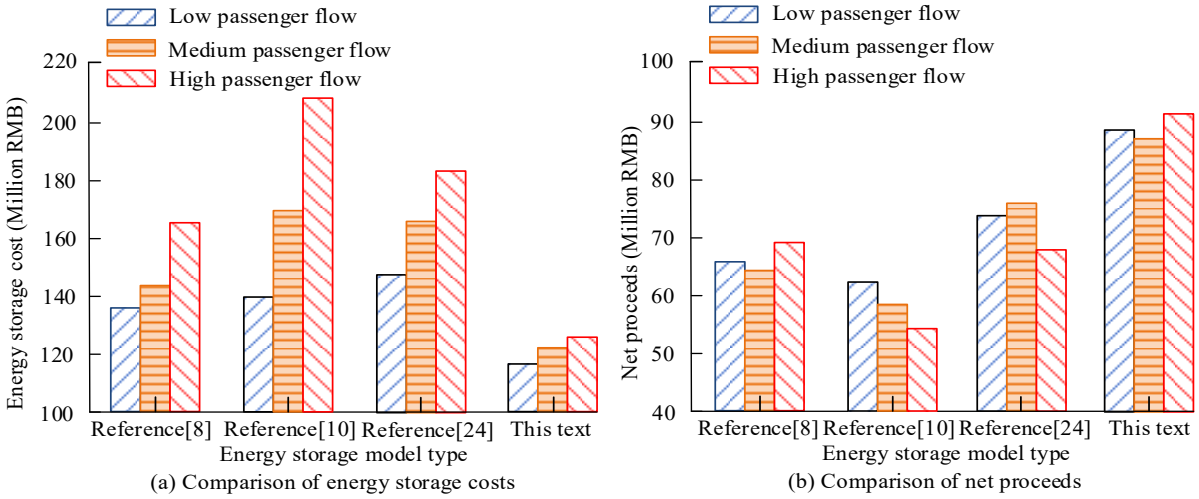

Figure 11. Economic comparison of RT-ESCS under different passenger flow rates

Figure 11(a) is the comparison of energy storage costs for various ESSs under different passenger flow rates. At all levels of passenger flow, the energy storage expenditure of the research model is the lowest. The model in reference [10] has relatively higher costs under high passenger flow, but lower costs under low passenger flow, indicating that it may be more suitable for low-demand environments. Comparing Figure 11(b), the net profit of the BAS-BP model also shows significant advantages, indicating that it can more accurately predict passenger flow and energy demand, thereby optimizing energy storage configuration, reducing energy storage costs, and optimizing energy usage efficiency and economic benefits. Finally, the scheduling optimization effects of different ESSs are compared, as listed in Table 4.

Table 4. Scheduling optimization effects of different ESSs

Energy storage type	Reference [8]	Reference [10]	Reference [24]	Research system	Percentage improvement (%)
Total scheduling cost ($\times 10^5$ RMB)	3.67	3.02	3.95	2.91	-17.95
Wind abandonment cost ($\times 10^5$ RMB)	1.52	1.35	1.04	0.96	-26.34
Photovoltaic abandonment cost ($\times 10^5$ RMB)	1.23	1.27	2.25	1.17	-26.11
Wind abandonment rate (%)	15.25	12.37	8.35	8.62	-28.11
Photovoltaic abandonment rate (%)	12.64	11.22	8.26	9.21	-13.98
Response speed (s)	15.28	21.29	17.38	11.46	-36.27

Comparing Table 4, the total scheduling cost of the research system is 2.91×10^5 yuan, which is an average reduction of 17.95% compared to other ESSs. It also shows better performance than other ESSs in terms of abandoned wind cost,

abandoned solar cost, and response speed, with an average reduction of 26.34% and 26.11% compared to other systems, and a response speed increase of 13.98%. The system in reference [24] performs the best in terms of curtailment rate but has poor performance in terms of energy storage cost and response speed. Taken together, day-ahead scheduling considers time-sharing tariffs and demand-side response, intra-day scheduling uses model predictive control to cope with the uncertainty of WASP generation, and real-time scheduling optimizes the train according to its real-time operating status. This hierarchical scheduling strategy optimizes the C&D process of the ESS, improves the energy utilization efficiency, and reduces the phenomenon of WASP abandonment, thereby achieving effective cost control and reduction on multiple time scales. In addition, the application of the improved multi-objective PSO algorithm improves the solving efficiency of the energy storage configuration model, which speeds up the process of scheduling plan development and reduces time consumption. Meanwhile, a reasonable SOC management strategy ensures that the battery and supercapacitor operate within a safe range, avoiding overcharging and over-discharging. This not only extends the service life of energy storage devices, reduces maintenance and replacement costs, but also helps maintain the stable operation of the system.

5. DISCUSSIONS

The stable operation of URT systems mainly relies on the efficient coordination of the power supply and ESS. In the context of extensive integration of RE, such as WASP, the uncertainty of its output and the time-varying characteristics of rail transit load can easily cause an energy supply-demand imbalance, thereby affecting the safety of train operation and the economic benefits of the system. Although traditional load forecasting methods and scheduling models have laid the foundation for energy management, they still have significant limitations in quickly responding to multisource disturbances and complex environmental changes. Therefore, there is an urgent need for a high-precision, robust, and adaptive intelligent prediction and scheduling model to provide a theoretical basis for energy coordination and regulation. Various methods have been proposed for optimizing energy dispatch in rail transit, such as predictive strategies based on linear programming. This strategy can quickly solve problems but has lower accuracy when dealing with nonlinear characteristics [25]. Rule-based control strategies are easy to implement but cannot respond to random fluctuations [26]. Although genetic algorithm optimization models have global search advantages, their convergence speed is slow and difficult to meet real-time scheduling requirements [27].

In summary, existing methods are difficult to meet the multiple demands of rail transit systems for prediction accuracy, response speed, and system robustness. Therefore, the study proposes an RT-ESCS system based on a BAS-BP prediction algorithm to achieve efficient, accurate, and stable energy management solutions. Compared to previous studies, this research has the following unique advantages: first, it aims to achieve precise modeling of complex nonlinear relationships by deeply integrating the BAS optimization algorithm with the BP network, thereby overcoming the efficiency bottleneck of high-dimensional search, such as the genetic algorithm. The second is the design of MTSES and a hybrid energy storage frequency management mechanism, which takes into account both low-frequency steady-state regulation and high-frequency transient response, effectively addressing the rigidity defects of the rule-based control strategy in stochastic fluctuation scenarios. The third is to construct a prediction configuration scheduling closed-loop collaborative framework, which enhances the overall reliability of the system through a dynamic feedback mechanism. This framework introduces data buffer compensation and step size adaptive technology to improve the system's fault tolerance for data anomalies and extreme working conditions. These innovations are not only theoretically significant but also provide more targeted and effective solutions for energy management in rail transportation in practical applications.

The current RT-ESCS system, based on the BAS-BP prediction algorithm, exhibits excellent performance; however, its practical application is fraught with challenges. At the algorithmic level, BAS-BP performs well in improving prediction accuracy and speed, while reducing MSE and time consumption; however, it also introduces the problem of increased complexity. Frequent adjustment of tentacle positions, calculation of fitness functions, and updating of network parameters increase computational resources, which can create performance bottlenecks when processing large-scale data. Therefore, it is necessary to find a balance between algorithm complexity and performance gains, and to explore optimization strategies that reduce resource consumption while maintaining efficient predictive ability. In addition, there is a trade-off between the performance gain and parameter sensitivity of the BAS-BP algorithm. Improper initial step size setting may slow down convergence speed and even result in local optima. In practice, the algorithm complexity and performance requirements should be balanced based on specific scenarios. When deployed in practice, data delay and signal loss in energy systems can have a significant impact on prediction and scheduling. Sensors and data acquisition devices in rail transit systems are susceptible to data transmission delays or signal loss due to environmental factors and equipment failures. This can degrade the quality of data input to the prediction model, which in turn affects the accuracy of the prediction. This study has not fully considered this issue. In the future, it is necessary to strengthen research on data collection and processing technology and utilize data buffering mechanisms and predictive compensation algorithms to mitigate latency losses and ensure the stable operation of the system. System responsiveness is crucial in the face of unpredictable load fluctuations or sensor failures. Although the energy storage configuration model has a certain degree of adaptability, it may not be able to respond in time in extreme cases. Future research needs to further optimize the control strategy to enhance the system's fault tolerance and robustness.

Meanwhile, different input uncertainties, such as weather anomalies and unexpected surges in demand, also pose challenges to system robustness. Abnormal weather conditions can significantly impact the power of wind power generation, and unexpected surges in demand may render the ESS unable to meet load demand within a short period.

Therefore, future research should construct more adaptive and resilient energy storage allocation models to cope with various uncertainties. By introducing advanced prediction algorithms and real-time monitoring technology, the system's responsiveness to unforeseeable conditions can be improved, ensuring stable operation in complex and changing real-world environments.

6. CONCLUSION

As the backbone network of urban transportation, the energy management and scheduling issues of the rail transit system are becoming increasingly prominent. To enhance the energy efficiency and economy of ESS, this study designed a prediction algorithm based on a BP network and introduced the BAS algorithm to optimize its parameters. The RT-ESCS model and MTSES optimization strategy were constructed. Experiments have shown that the BAS-BP algorithm predicts photovoltaic output results that are closest to actual power generation, and its prediction accuracy is significantly improved compared to the unoptimized BP algorithm. At the same time, the BAS-BP algorithm exhibited a positive optimization iteration effect, with MSE values of 36.57% and 40.18% for photovoltaic and wind power prediction, respectively, which significantly improved the prediction accuracy compared to other algorithms. Moreover, its time consumption for photovoltaic and wind power prediction has been reduced by 29.95% and 33.21% compared to other algorithms. In addition, the research model accurately predicted passenger flow and energy demand, with a total scheduling cost of 2.91×10^5 yuan, representing an average reduction of 17.95% compared to other systems. The cost of abandoning WASP has decreased by 26.34% and 26.11% compared to other systems, and the response speed has increased by 13.98%. The results show that the BAS-BP algorithm significantly improves the prediction accuracy of wind power generation and combined with the hybrid ESS frequency division management strategy, effectively extends the life of energy storage equipment and reduces overall costs. At the same time, the MTSES scheme, while ensuring power supply reliability, further improves system response speed and energy utilization efficiency through dynamic optimization of C&D scheduling. The study ensures the reproducibility of the simulations through the use of measured data, standardized parameter configurations, a comprehensive algorithm description, and detailed implementation details.

However, the study still suffers from the following limitations: first, the model's adaptability to complex physical environments is yet to be verified. For example, the impact of extreme temperatures and humidity on the performance of energy storage devices, as well as capacity degradation due to device aging, has not been included in the quantitative analysis. Second, the real-time performance of the algorithm is limited by the response delay of the data acquisition hardware, especially in the case of multi-node cooperative scheduling, which may reduce the global optimization efficiency due to communication bottlenecks. Third, the current prediction model does not deeply integrate the multi-dimensional dynamic information of the train operating environment, resulting in insufficient scheduling robustness under extreme scenarios. Future research will focus on three aspects of improvement: The first is to build a data physical fusion digital twin platform, integrating real-time sensor compensation algorithms and device health status monitoring modules to enhance fault tolerance in the event of data loss or anomalies. The second is to design a lightweight edge computing architecture through the distributed deployment of the BAS-BP model, thereby reducing the computing load of the central server and realizing the privacy protection and collaborative optimization of cross-line ESS by combining federated learning technology. The third is to introduce a spatiotemporal attention mechanism and multimodal data fusion technology, embedding dynamic parameters such as track slope, vehicle load, and weather warning in the prediction model. This can enhance decision-making adaptability under complex working conditions, explore cross-system energy interaction strategies with urban power grids and distributed photovoltaics, and promote the evolution of rail transit energy storage towards key nodes in smart city energy networks.

ACKNOWLEDGEMENT

The research is supported by the Qing Lan Project.

CONFLICT OF INTEREST

The authors declare no conflicts of interest

AUTHORS' CONTRIBUTION

L. Han: Conceptualization, Methodology, Software, Validation, Formal Analysis, Investigation, Resources, Data Curation, Writing – Original Draft, Review & Editing, Supervision, Project Administration

L. Yang: Conceptualization, Validation, Funding Acquisition

L. Su: Visualization, Validation

REFERENCES

[1] L. Jin, Q. Meng, and S. Liang, "Model of a composite energy storage system for urban rail trains," *Computer Systems Science and Engineering*, vol. 40, no. 3, pp. 1145‑1152, 2022.

[2] R. A. A. Khalil, "Building the public transportation system in Libya," *Engineering Heritage Journal*, vol. 8, no. 1, pp. 7-12, 2024.

[3] C. Chong, M. J. Li, and Y. Z. Tian, "Decarbonization-oriented rail transportation and renewable energy integration development configurations, solutions, and enabling/empowering technologies," *Transactions of China Electrotechnical Society*, vol. 38, no. 12, pp. 3321-3337, 2023.

[4] T. Boonlert, K. Hongesombut, and M. Watanabe, "Optimal tuning of virtual inertia-integrated railway power conditioner with phase correction for renewable-dominated supplies with V/V transformers," *IEEE Access*, vol. 12, no. 7, pp. 125266-125283, 2024.

[5] Z. Wu, Y. Zhao, and N. Zhang, "A literature survey of green and low-carbon economics using natural experiment approaches in top field journal," *Green and Low-Carbon Economy*, vol. 1, no. 1, pp. 2-14, 2023.

[6] S. Xia, H. Wu, Y. Mao, T. Wu, G. Song, J. S. Terzic, and M. Shahidehpour, "Photovoltaic power generation and energy storage capacity cooperative planning method for rail transit self-consistent energy systems considering the impact of DoD," *IEEE Transactions on Smart Grid*, vol. 16, no. 1, pp. 665-677, 2024.

[7] K. Xu, C. Shen, C. Xu, L. Fan, H. Huo, J. Xu, and L. Cui, "Modeling and control-oriented thermal characteristics under variable load of the solid oxide fuel cell," *Journal of Solid-State Electrochemistry*, vol. 27, no. 8, pp. 2083-2099, 2023.

[8] Y. Liu, Z. Yang, X. Wu, D. Sha, F. Lin, and X. Fang, "An adaptive energy management strategy of stationary hybrid energy storage system," *IEEE Transactions on Transportation Electrification*, vol. 8, no. 2, pp. 2261-2272, 2022.

[9] H. Dong, Z. Tian, J. W. Spencer, D. Fletcher, and S. Hajiabady, "Coordinated control strategy of railway multisource traction system with energy storage and renewable energy," *IEEE Transactions on Intelligent Transportation Systems*, vol. 24, no. 12, pp. 15702-15713, 2023.

[10] J. Yuan, K. Cheng, and K. Qu, "Optimal dispatching of high-speed railway power system based on hybrid energy storage system," *Energy Reports*, vol. 8, no. 4, pp. 433-442, 2022.

[11] Y. Chen, M. Chen, Z. Liang, and L. Liu, "Dynamic voltage unbalance constrained economic dispatch for electrified railways integrated energy storage," *IEEE Transactions on Industrial Informatics*, vol. 18, no. 11, pp. 8225-8235, 2022.

[12] B. Xu, Z. Yan, W. Zhou, L. Zhang, H. Yang, Y. Liu, and L. Liu, "A bidirectional integrated equalizer based on the SEPIC-Zeta converter for hybrid energy storage system," *IEEE Transactions on Power Electronics*, vol. 37, no. 10, pp. 12659-12668, 2022.

[13] X. Li, J. Wang, and C. Yang, "Risk prediction in financial management of listed companies based on optimized BP neural network under digital economy," *Neural Computing and Applications*, vol. 35, no. 3, pp. 2045-2058, 2023.

[14] E. Liu, J. Li, A. Zheng, H. Liu, and T. Jiang, "Research on the prediction model of the used car price in view of the PSO-GRA-BP neural network," *Sustainability*, vol. 14, no. 15, pp. 8993-9006, 2022.

[15] H. Bai, Z. Chu, D. Wang, Y. Bao, L. Qin, Y. Zheng, and F. Li, "Predictive control of microwave hot-air coupled drying model based on GWO-BP neural network," *Drying Technology*, vol. 41, no. 7, pp. 1148-1158, 2023.

[16] Y. Deng, Z. Weng, and T. Zhang, "Metaverse-driven remote management solution for scene-based energy storage power stations," *Evolutionary Intelligence*, vol. 16, no. 5, pp. 1521-1532, 2023.

[17] Q. Ma, Z. J. Yang, P. Luo, Z. Lei, and Q. Guo, "A rolling-adaptive peak clipping control strategy coordinating RBE recycling and PV consumption," *IEEE Transactions on Intelligent Transportation Systems*, vol. 24, no. 4, pp. 4348-4363, 2023.

[18] A. A. Abdalla, M. S. El Moursi, T. H. El-Fouly, and K. H. Al Hosani, "A novel adaptive power smoothing approach for PV power plant with hybrid energy storage system," *IEEE Transactions on Sustainable Energy*, vol. 14, no. 3, pp. 1457-1473, 2023.

[19] L. Hu, W. Wang, and G. Ding, "RUL prediction for lithium-ion batteries based on variational mode decomposition and hybrid network model," *Signal, Image and Video Processing*, vol. 17, no. 6, pp. 3109-3117, 2023.

[20] X. Luo, Q. Guo, Y. Tian, J. Cao, and G. Luo, "Remote sensing inversion model of water quality parameters based on BP neural network and spatial distribution analysis in the middle reaches of the Yangtze River basin in China," *Journal of the Indian Society of Remote Sensing*, vol. 53, no. 8, pp. 2535-2557, 2025.

[21] B. Qiu, K. Feng, and Y. Wang, "An improved Beetle Antennae Search algorithm of solving inverse kinematics of quadruped robot," *Jixie Kexue Yu Jishu/ Mechanical Science and Technology for Aerospace Engineering*, vol. 44, no. 4, pp. 601-608, 2025.

[22] H. Su, J. Liu, A. Liu, and B. Li, "A study of an active noise control system with continuous tracking of the human ear and noise segmentation control," *International Journal of Automotive Technology*, vol. 26, no. 4, pp. 929-945, 2025.

[23] C. Lu and H. Du, "Improved RRT trajectory planning method based on tower model and bidirectional beetle antennae search algorithm," *Kongzhi yu Juece/Control and Decision*, vol. 40, no. 3, pp. 955-962, 2025.

[24] Y. X. Liu, Y. B. Chen, H. X. Tian, J. Q. Li, Y. T. Li, and L. Chun, "New energy and energy storage planning configuration in rail transportation self-consistent energy systems based on two-stage robust optimization," High Voltage Engineering, vol. 50, no. 10, pp. 4713-4723, 2024.

[25] S. Wu, J. Wu, Y. Sun, and T. Yao, "Optimization algorithm for urban rail transit operation scheduling based on linear programming," *Scalable Computing: Practice and Experience*, vol. 24, no. 3, pp. 203-216, 2023.

[26] Z. Zhong, J. Mi, Y. Zhao, Z. Yang, and F. Lin, "Coordinated control of the onboard and wayside energy storage system of an urban rail train based on rule mining," *Urban Rail Transit*, vol. 10, no. 3, pp. 232‑247, 2024.

[27] H. J. Kaleybar, M. Davoodi, M. Brenna, and D. Zaninelli, "Applications of genetic algorithm and its variants in rail vehicle systems: A bibliometric analysis and comprehensive review," *IEEE Access*, vol. 11, no. 9, pp. 68972‑68993, 2023.